

GAS DISCHARGES, PLASMA

Scaling Laws for the Spatial Distributions of the Plasma Parameters in the Positive Column of a DC Oxygen Discharge

E. A. Bogdanov*, A. A. Kudryavtsev*, L. D. Tsendin**, R. R. Arslanbekov***, V. I. Kolobov***, and V. V. Kudryavtsev****

* St. Petersburg State University, Universitetskaya nab. 7/9, St. Petersburg, 199034 Russia
e-mail: akud@ak2138.spb.edu

** St. Petersburg State Technical University, ul. Politekhnikeskaya 29, St. Petersburg, 195251 Russia

*** CFD Research Corporation, 215 Wynn Drive, Huntsville, AL, USA

**** CFD-Canada, 45 English Ivyway, Toronto, Canada

Received March 4, 2003

Abstract—Comprehensive self-consistent simulations of the positive column plasma of a dc oxygen discharge are performed with the help of commercial CFDRC software (<http://www.cfdrc.com/~cfdplasma>), which enables one to carry out computations in an arbitrary 3D geometry using fluid equations for heavy components and a kinetic equation for electrons. The main scaling laws for the spatial distributions of charged particles are determined. These scaling laws are found to be quite different in the parameter ranges that are dominated by different physical processes. At low pressures, both the electrons and negative ions in the inner discharge region obey a Boltzmann distribution; as a result, a flat profile of the electron density and a parabolic profile of the ion density are established there. In the ion balance, transport processes prevail, so that ion heating in an electric field dramatically affects the spatial distribution of the charged particles. At elevated pressures, the volume processes prevail in the balance of negative ions and the profiles of the charged particle densities in the inner region turn out to be similar to each other. © 2003 MAIK “Nauka/Interperiodica”.

Interest in discharges in electronegative gases stems from their wide use in modern plasma technologies [1]. In order to predict the possible parameter distributions and their dependence on the external conditions, considerable attention is paid to elucidating the relations between the main plasma parameters. Various aspects of this problem as applied to electronegative gases were considered by many research groups (see, e.g., [1–26]). It was found that, in the presence of negative ions, the processes of spatial transport, which determine the density profiles and other plasma parameters, possess a number of specific features [26]. Knowledge of the spatial distributions of charged particles is of crucial importance for understanding and optimizing the operation of various devices and technologies, such as ion sources and facilities for the plasma treatment of materials. Early attempts to reduce the problem to a set of ambipolar diffusion coefficients by using simplified models [2–9] were contradictory and there were no criteria for their applicability. In [10–12], it was shown that a specific feature of an electronegative-gas plasma is that it stratifies into regions with different ion compositions. In the outer region (shell) of such a plasma, negative ions are practically absent (Figs. 1–3), because they are drawn by the electric field into the plasma interior. Although the thickness of this shell is usually small, its presence is of fundamental importance because it confines the negative ions inside the plasma volume. As a result, the flux of negative ions to the wall

is practically absent (in contrast to those of electrons and ions). In such a situation, the only means to extract negative ions from the discharge is to apply an accelerating voltage U to the wall (or an extracting electrode). The magnitude of this voltage should be large enough for the space charge layer produced at the plasma boundary to extend to the inner region containing negative ions. The thicker the shell, the higher voltage ($U \sim$

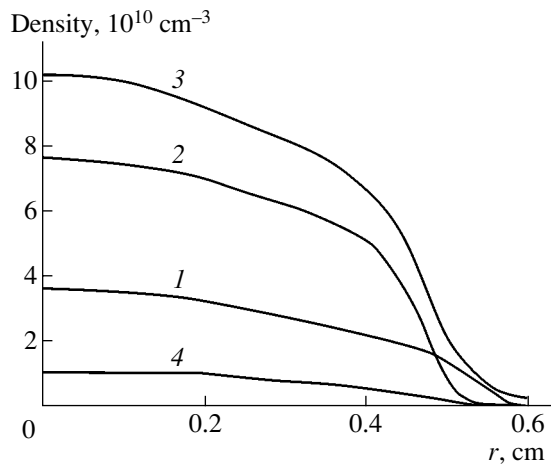


Fig. 1. Profiles of the charged particle densities for $p = 1$ torr and $I = 50$ mA: (1) n_e , (2) n_n , (3) n_p , and (4) $n[\text{O}^+]$.

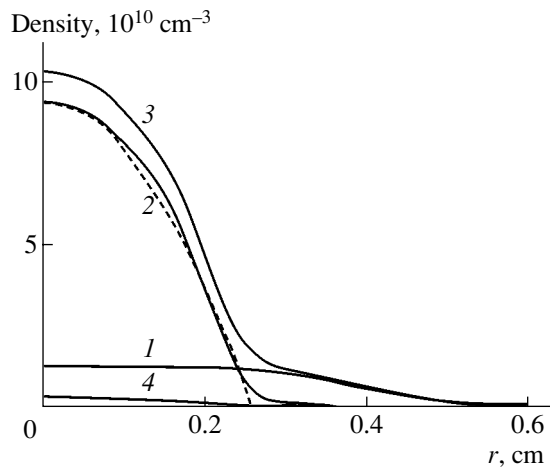


Fig. 2. Same as in Fig. 1 for $p = 0.15$ torr without allowance for ion heating: (1) n_e , (2) n_n , (3) n_p , and (4) $n[\text{O}^+]$. The dashed curve shows parabolic distribution (18).

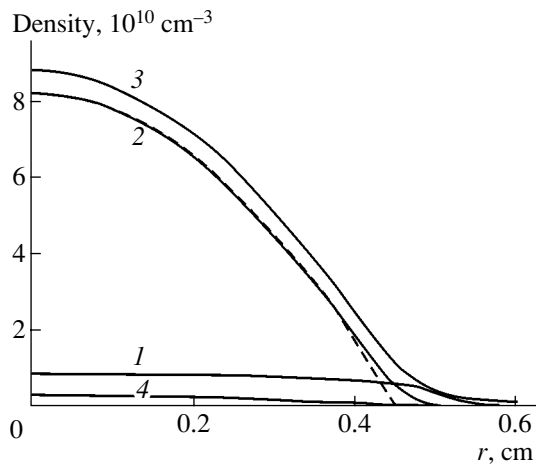


Fig. 3. Same as in Fig. 2, but with allowance for ion heating.

$L_{\text{sh}}^{2/3}$) that must be applied to enable the flux of negative ions to the wall.

Besides its practical importance, oxygen plasma is also an important test object [16]. The peculiar features of the spatial distributions of the oxygen plasma parameters have been the subject of a heated discussion. Thus, in [16–18], it was pointed out that using a Boltzmann distribution from [4] for not only electrons but also negative ions (as was done in [13–15]) is unjustified. It is alternatively asserted in [16–18] that the densities of charged particles in such a plasma should be proportional to each other [10–12]. In [24], it was shown that, depending on conditions, both types of distribution can occur. For example, we observed a transition from one type of the above profiles to another as the pressure was reduced (see below).

To verify the functional relations between the plasma parameters obtained with the help of simplified

models, they should be compared with the results of full-scale numerical simulations. Such simulations should be based on self-consistent models that take into account spatial transport processes and volume plasmochemical reactions. Such an attempt was made by us in [27], in which we compared the results of kinetic and fluid simulations of the positive column plasma of a dc oxygen discharge by using commercial CFDRC software [28]. A two-temperature (2T) fluid model was proposed, which allowed us to incorporate kinetic effects in the conventional fluid model in the simplest way.

Here, we continue the study of [27]; specifically, we investigate the features of the spatial distributions of the plasma parameters in the positive column of a dc discharge in a 12-mm-diameter glass tube at pressures of 0.05–3 torr and discharge currents of 5–200 mA. These conditions correspond to those in [21, 22], in which, in our opinion, one of the most detailed experimental and theoretical studies of the positive column of a dc oxygen discharge were reported.

The discharge was simulated by using a commercial software developed at the CFD Research Corporation (Huntsville, AL, USA) [28]. A detailed self-consistent model of the discharge plasma, numerical iteration scheme, and technique for solving the set of equations are described in [28]. The density and mean energy of the electron component can be obtained by solving either fluid balance equations or the kinetic equation for the electron distribution function (EDF). The self-consistent electric field is found from Poisson's equation. Heavy particles are described in the fluid model. Both the analytic results and the published data show that, in the parameter range under study, the neutral gas is heated to no higher than 50–150 K. Such an increase in the gas temperature T results merely in a decrease in the gas density. Since this is of minor importance for our problem, the gas temperature was assumed to be equal to room temperature and constant over the discharge cross section. On the other hand, the ion temperature can increase significantly, particularly at low pressures [20, 21]. As the pressure decreases, the reduced electric field E/p increases, so that the directed velocity acquired by the ions in this field can become higher than the random (thermal) velocity [29]. The coefficient of ion diffusion also increases. This can dramatically change the ion density profiles [20]. Model calculations with allowance for ion heating in a longitudinal electric field show that the outer region occupied by the electron-ion plasma shrinks and can even completely disappear [20, 21]. Ion heating also leads to a decrease in the detachment rate constant and, consequently, to an increase in the relative density of negative ions n_n/n_e (the degree of electronegativity) [21].

Here, we do not present the list of the volume plasmochemical reactions involved because it is the same as in [27]. Note only that we solved the balance equations for the vibrationally excited states $\text{O}_2(v)$ ($v = 0, 1$)

of an oxygen molecule and the electronically-excited states of an oxygen molecule ($O_2(X^3\Sigma_g^-)$, $O_2(a^1\Delta)$, $O_2(b^1\Sigma)$, and $O_2(Ry)$); oxygen atom ($O(^3P)$, $O(^1S)$, and $O(^1D)$); ozone molecule O_3 ; and O^+ , O_2^+ , O_4^+ , O^- , O_2^- , and O_3^- ions with allowance for 160 plasmachemical reactions between them.

Typical ion density profiles computed for the gas pressure $p = 1$ torr are shown in Fig. 1, and those computed for $p = 0.15$ torr without and with allowance for ion heating in the longitudinal electric field are shown in Figs. 2 and 3, respectively. Ion heating [20–22] was calculated by the formulas for the effective transverse ion temperature [29]

$$T_i^\perp = T + \frac{(M_i + M)Mw^2}{3(2M + M_i)}, \quad (1)$$

where M and M_i are the masses of a molecule and an ion, respectively, and w is the ion drift velocity in the longitudinal electric field E_z .

For example, at $p = 1$ torr, the transverse ion temperature is $T_i^\perp \approx 760$ K, whereas at $p = 0.15$ torr, it is $T_i^\perp \approx 5200$ K. For oxygen, an order of magnitude of the ion temperature as a function of the parameter $p\Lambda$ is presented, e.g., in [21, Fig. 5].

It can be seen from Figs. 1–3 that the spatial distribution of the charged particle densities is highly non-uniform over the discharge cross section. Almost all of the negative ions reside in the inner ion–ion plasma region (which will be marked by subscript 0). The radius of this region is $r = r_0$. The outer electron–ion plasma region ($r_0 < r < R$) (subscript 1) consists of electrons and positive ions, whereas the negative ions are practically absent there. A comparison of the profiles presented in Figs. 2 and 3 show that taking into account ion heating (which increases the ion diffusion coefficient) dramatically changes the shell thickness. For this reason, when analyzing the spatial profiles of the charged particle densities in electronegative gases, one of the central problems is the problem of the ion temperature [20, 21].

The main positive ion is O_2^+ and the main negative ion is O^- . The densities of all other ions are small compared with the densities of these ions. Hence, for the sake of qualitative analysis, it is sufficient to consider a plasma consisting of only electrons, positive ions, and negative ions (subscripts e , p , and n , respectively).

To explain the dependences observed and predict how they are affected by the external conditions, we consider, as in [1–26], the conventional set of drift–diffusion equations

$$-D_p \nabla (\nabla n_p + kn_p \nabla n_e/n_e) = v_i n_e - K_r n_n n_p, \quad (2)$$

$$-D_n \nabla (\nabla n_n - kn_n \nabla n_e/n_e) = v_a n_e - v_d n_n - K_r n_n n_p, \quad (3)$$

$$n_p = n_n + n_e. \quad (4)$$

with a Boltzmann distribution for the electrons: $E = -T_e \nabla n_e/n_e$. Here, v_i , v_a , and v_d are the ionization, attachment, and detachment frequencies, respectively; K_r is the rate constant for ion–ion recombination; and $k = T_e/T_i$ is the electron-to-ion temperature ratio. The boundary conditions for the set of Eqs. (2) and (3) are [1, 26]

$$\begin{aligned} \nabla n_n = \nabla n_p = 0 \quad \text{at} \quad r = 0, \\ n_n = n_p = \nabla n_n = 0 \quad \text{at} \quad r = R. \end{aligned} \quad (5)$$

Since the flux of negative ions to the wall is zero, we find from Eq. (3) that the densities averaged over the cross section (\bar{n}) satisfy the relationship [1, 26]

$$v_a \bar{n}_e = v_d \bar{n}_n + K_r \bar{n}_n \bar{n}_p. \quad (6)$$

In further analysis, we will mainly follow [24–27]. We divide Eqs. (2) and (3) by the corresponding diffusion coefficients and sum them up. As a result, we arrive at the equation [10, 26]

$$-2\Delta n_n/k - \Delta n_e = n_e/l_e^2 - 2n_n/k l_n^2, \quad (7)$$

which is of fundamental importance for analyzing the solution to the set of Eqs. (2) and (3). Equation (7) contains two characteristic space scales, l_e and l_n , which are defined by

$$\begin{aligned} 1/l_e^2 &= 1/l_{ion}^2 + 1/l_a^2 = v_i/D_{ap} + v_a/D_{an} \\ &= \tau_{ap} v_i/\Lambda^2 + \tau_{an} v_a/\Lambda^2, \end{aligned} \quad (8)$$

$$\begin{aligned} 1/l_n^2 &= 1/l_{nd}^2 + 1/l_{nr}^2 = v_d/2D_n + n_p K_r/D_{np} \\ &= \tau_n v_d/\Lambda^2 + \tau_{np} K_r n_p/\Lambda^2, \end{aligned} \quad (9)$$

where $D_{an, ap} = D_{n, p}(k + 1)$ and $D_{np} = 2D_n D_p/(D_n + D_p)$ are the coefficients of electron–ion and ion–ion ambipolar diffusion, respectively; $\tau_j = \Lambda^2/D_j$ are the corresponding characteristic times; and Λ is the diffusion length, which, in the case of cylindrical geometry, is equal to $\Lambda = R/2.4$. Figure 4 shows, as an example, the calculated lengths (8) and (9) versus the parameter $p\Lambda$ for oxygen.

Since the ambipolar electric field draw negative ions into the plasma, their density in the outer region ($r_0 \leq r \leq R$) is low, $n_n(r) \approx 0$; hence, we have $n_e(r) \approx n_p(r)$ in this region. Neglecting the terms with n_n , we can write Eq. (7) in the form

$$-\Delta n_e = n_e/l_e^2.$$

Taking into account the spread caused by ion diffusion, we find that the thickness of the outer region satisfies the condition $R - r_0 \leq l_e$; i.e., l_e determines the maximum thickness of the shell. Under our conditions, this thickness is small compared with the tube radius R (and, hence, with the characteristic diffusion length $\Lambda =$

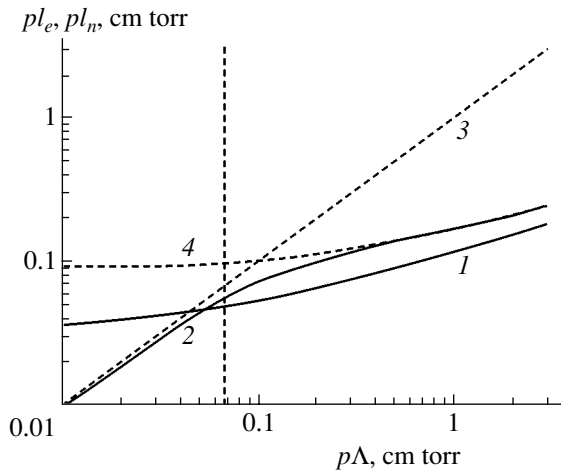


Fig. 4. Characteristic lengths l_n (1) and l_e (2) vs. parameter $p\Lambda$ for an oxygen discharge. The asymptotes for l_e , $l_e \approx \Lambda$ (3) and $l_e \approx l_n \sqrt{T_e/2T_i}$ (4) are also shown.

$R/2.4$). Therefore, the outer region I can be treated in plane geometry. Then, for the plasma density profile in the region $r_0 \leq r \leq R$, we can use the solution [10, 24–26]

$$n_e(r) = n_e(r_0) \sin(\pi(R-r)/2l_e) / \sin(\pi(R-r_0)/2l_e). \quad (10)$$

The density profiles in the inner region 0 depend substantially on the ratio between R and l_n (see Eq. (9)), i.e., between the radius and the distance a negative ion covers due to diffusion during its lifetime with respect to volume processes [24–26]. At $\tau_{an}v_a > 1$, length l_e (8) is small ($l_e < \Lambda$), and, under typical discharge conditions ($\bar{n}_n/\bar{n}_e < k \approx 100$), length l_n turns out to be even smaller ($l_n < l_e$); hence, ion diffusion can be ignored [10–12]. When the opposite inequality is satisfied ($\tau_{an}v_a < 1$), the electron–ion plasma occupies almost the entire cross section of the tube, whereas length l_n can be either longer or shorter than the radius of the inner ion–ion region. Hence, to obtain functional dependences in the inner region, it is reasonable to consider two limiting regimes with large and small values of the parameter $\tau_{an}v_a$. Since this parameter is quadratic in pressure, the boundary between these regimes ($\tau_{an}v_a = 1$) can be determined with sufficient accuracy. For oxygen, the boundary value of this parameter corresponds to $p\Lambda \approx 0.07$ cm torr (the dashed vertical line in Fig. 4), so that $\tau_{an}v_a > 1$ at $p\Lambda > 0.07$ cm torr and vice versa. Consequently, length l_e (8) has two asymptotes: $l_e \approx \Lambda$ at low pressures, $p\Lambda < 0.07$ cm torr, and $l_e \approx l_n \sqrt{T_e/2T_i}$ in the opposite case (Fig. 4).

At high attachment frequencies ($\tau_{an}v_a > 1$), characteristic lengths (8) and (9), as was mentioned above, are both small ($l_n < l_e < \Lambda$) (Fig. 4). Since $l_n < l_e$, we can neglect ion diffusion in Eqs. (2) and (3) (as was done in

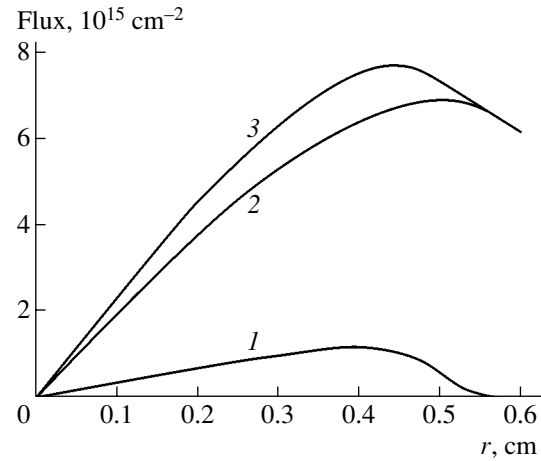


Fig. 5. Contributions of spatial transport and volume processes to the negative ion balance for $p = 1$ torr and $I = 50$ mA. Curve 1 shows the flux of negative ions (with a minus sign), curve 2 shows the total production of ions, and curve 3 shows the ion loss.

[10–12]) and assume that the shell thickness is $R - r_0 \approx l_e$ (i.e., the denominator in Eq. (10) is equal to unity). In the case at hand, in balance equation (3) for negative ions, their transport is insignificant as compared to volume processes (see Fig. 5), so that the negative ion flux is almost completely determined by the drift component. Hence, at $n_p \approx n_n > n_e$, the fluxes of positive and negative ions in the inner region are almost the same in magnitude, but opposite in sign; i.e., we have [10, 26]

$$\Gamma_n/b_n \approx kn_p \nabla n_e/n_e \approx kn_n \nabla n_e/n_e \approx -\Gamma_p/b_p. \quad (11a)$$

For this reason, in Eq. (7), in which these fluxes are summed up, they almost completely cancel each other in the inner ion–ion region. In other words, at $r < r_0$, the terms on the left-hand side of Eq. (7) (which are responsible for spatial transport) are small compared to the terms on the right-hand side (which are responsible for volume processes). Hence, the local balance of the volume plasmochemical processes resulting in the production and loss of ions, $n_e/l_e^2 = 2n_n/kl_n^2$, holds with a high accuracy. At $\tau_{an}v_a > 1$, the following important relation can be deduced from this equality [10, 24–26]:

$$\begin{aligned} (v_i/D_p + v_a/D_n)n_e &= v_d n_n/D_n \\ &+ K_r n_n(n_n + n_e)/(1/D_p + 1/D_n), \end{aligned} \quad (12a)$$

which allows one to obtain the relationships between the plasma parameters in the central region $r < r_0$.

The relationships between the densities of charged particles depend on the mechanism responsible for the loss of negative ions, i.e., on the relationship between the terms on the right-hand side of Eq. (12a). At $\tau_{an}v_a > 1$, the loss of negative ions in an oxygen plasma is governed by detachment processes (the detachment regime with $v_d > n_p K_r$) and their recombination can be neglected. Then, it follows from Eq. (12a) that the pro-

files of the electron and negative ion densities are similar to each other,

$$\nabla n_e/n_e = \nabla n_n/n_n, \quad n_e(x)/n_n(x) = \text{const.} \quad (12b)$$

This condition was first proposed in [2] and then was justified in [10–12], assuming that ion diffusion can be neglected as compared to ion drift. It follows from the above analysis that Eq. (12b) is valid only at $\tau_{an}v_a > 1$; hence, extrapolating it to the low pressure range [16–18] is incorrect. The validity of Eq. (12b) for oxygen is illustrated in Fig. 6, which shows the density profiles from Fig. 1 ($p = 1$ torr) normalized to the central electron density. Substituting Eq. (12b) into Eq. (2) or (3), we find that, with a significant degree of electronegativity ($n_n > n_e$), the densities in the inner region satisfy the relationship

$$n_p(r) \sim n_n(r) \sim n_e(r) \sim J_0(r/l_0). \quad (13a)$$

For plane geometry, the Bessel function should be replaced with $\cos(x/l_0)$. In Eq. (13a), the characteristic length [10, 26]

$$l_0^2 = \frac{D_{an}}{v_d} + \frac{v_a D_{ap}}{v_i v_d} \approx \frac{\Lambda^2 \bar{n}_n}{v_i \tau_{ap} \bar{n}_e} > \Lambda^2 \quad (13b)$$

also determines the ambipolar electric field ($E(r) = -T_e \nabla n_e/n_e$) in the central region ($r < r_0$):

$$E^{(0)}(r) \approx -T_e J_1(r/l_0)/l_0 \approx -T_e r/l_0^2. \quad (14a)$$

Since the conditions $l_0 > \Lambda > l_e$ are usually satisfied, density profiles (13a) in the inner region are flatter than in the outer region, and, when they are extended up to the wall, they do not turn to zero (see Eq. (5)). Consequently, field (14a) is weaker than the electric field in the shell ($r_0 < r < R$), for which we have from Eq. (10) the following estimate:

$$E^{(1)}(r) \approx -\frac{\pi T_e}{2l_e} \cot \frac{\pi(R-r)}{2l_e} \approx -\frac{\pi^2 T_e}{2l_e^2} (r-r_0). \quad (14b)$$

To illustrate the limiting cases, we use Eqs. (2) and (3) to rewrite relationship (11a) in the form [10, 26]

$$\Gamma_n = v_a \int_{r_0}^R n_e(r) r dr = -\Gamma_p D = D v_i \int_0^{r_0} n_e(r) r dr, \quad (11b)$$

where $D = (D_n/D_p) \sim 1$. This relationship means that the number of ions that undergo attachment in the outer region is equal to the number of ions produced in the central region due to ionization. In the thin shell, a comparatively small flux of negative ions Γ_n is produced due to attachment; hence, a fairly weak electric field (14a) is sufficient to transport these ions into the inner region, in which they disappear due to detachment. Since, at $\tau_{an}v_a > 1$, the electrons in the inner region disappear mainly due to attachment, it is necessary to enable just a minor flux of positive ions toward the

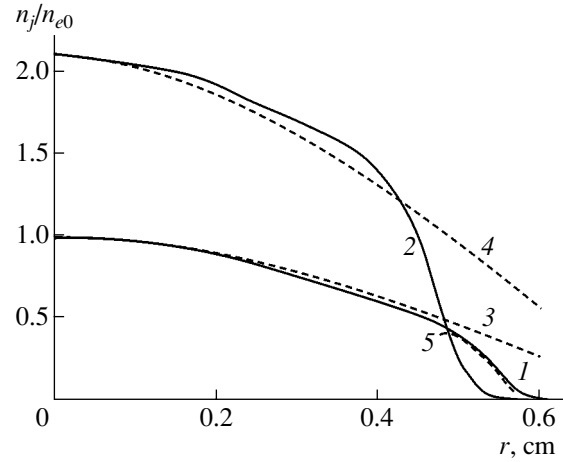


Fig. 6. Normalized density profiles for $p = 1$ torr and $I = 50$ mA: (1) $n_e(r)/n_{e0}$, (2) $n_n(r)/n_{e0}$. Curves 3 and 4 show the results calculated by formula (13), and curve 5 shows profile (10) in the outer region.

outer region. In other words, relationship (11b) means that, if the local plasmachemical balance of ions dominates over their spatial transport, the latter should only compensate for a relatively small difference between the attachment and detachment of negative ions.

Using expression (10) for $n_e(r)$ and Eqs. (14), we can obtain from Eq. (11b) the ionization frequency v_i , which represents the eigenvalue of the boundary value problem described by Eqs. (2) and (3) [26]. The simple estimate $\Gamma_n \approx v_a n_e l_e \approx \bar{\Gamma}_p \approx v_i n_e \Lambda$ gives $v_i \approx n_e l_e / \Lambda \approx \sqrt{v_a / \tau_{an}}$ [10, 26]. In the case at hand, we have $v_i \tau_{an} \approx \sqrt{v_a \tau_{an}} > 1$; hence, we obtain $\tau_{an} v_i > 1$. This means that the ionization frequency exceeds the value given by the Schottky formula for a simple plasma ($\tau_{an} v_i = 1$) [25, 26].

The density of the negative ions that are produced in the shell due to attachment can be deduced from their flux Γ_n (11b):

$$n_n \approx \Gamma_n / b_n E^{(1)} \approx \frac{8 l_e^2 n_e(r_0)}{\pi^2 D_{an}} \sin^2 \frac{\pi(R-r)}{2l_e} \tan \frac{\pi(R-r)}{2l_e}. \quad (15)$$

This density is much lower than the densities of electrons and positive ions,

$$n_n \approx \frac{\pi n_e(r_0) v_a}{4 D_{an} l_e} (r-R)^3 \quad (r_0 < r \leq R). \quad (15a)$$

At the point $r = r_0 \approx R - l_e$, the field $E^{(1)}$ is close to zero, whereas the flux Γ_n (11b), caused by attachment in the outer region, is finite. Therefore, when approaching the point $r = r_0$, negative ion density (15) sharply

increases,

$$n_n \approx \frac{8l_e^3 n_e(r_0) v_a}{\pi^3 D_{an}(r-r_0)} \quad (r \geq r_0 = R - l_e), \quad (15b)$$

to its value in the inner region, which is determined by Eq. (12). The transition zone separating regions 0 and 1 with different ion compositions is narrow ($\sim l_n < l_e$). For this reason, it was treated in [10, 26] as a diffusive jump in which ion densities undergo a break, whereas the ion fluxes and the electron density are continuous. The validity of relationship (12) in the region $r < r_0$ in an oxygen discharge is illustrated in Fig. 6, which shows the normalized density profiles obtained from the profiles in Fig. 1 at a pressure of $p = 1$ torr. The dashed curves in Fig. 6 show the profiles calculated by formula (13) for the inner region and by formula (10) for the shell with the thickness $R - r_0 \approx l_e$. When deducing formula (10) for the outer region, the shell thickness δ_{sh} was taken into account; i.e., it was assumed that the electron density vanished at $r = R - \delta_{sh}$, rather than at the tube wall. It can be seen that the results of calculations by these formulas agree well with the results of full-scale simulations.¹

At lower pressures, the role of spatial transport increases and, thus, the characteristic length l_e (8) and l_n (9) also increase. The increase in length l_0 (13b) leads to the flattening of density profiles (13a) in the inner region. Because of the increase in the length l_n , the region with a sharp change of the ion density spreads out due to ion diffusion; hence, the transient region can no longer be treated as a jump. As a result, the ion density profiles become bell-shaped.

At $l_n \geq \Lambda$, the negative ions are able to pass throughout the entire discharge volume due to their diffusion. However, they turn out to be trapped in the inner region by the electric field; as a result, a Boltzmann distribution (similar to that for electrons) is established:

$$-T_e \nabla n_e / n_e = -T \nabla n_n / n_n = E. \quad (16)$$

It follows from Eqs. (8) and (9) that, generally, the self-diffusion of negative ions prevails ($l_n > \Lambda$) only when attachment is insignificant as compared to the ambipolar diffusion of negative ions (ion diffusion with the electron temperature), i.e., when $\tau_{an} v_a \ll 1$ (see [24–26] for details).

Condition (16) leads to the relationship

$$n_e(r) / n_e(0) = [n_n(r) / n_n(0)]^{1/k}, \quad (17)$$

¹ Note that, for the recombination regime ($v_d < n_p K_p$), it follows from Eqs. (11a) and (12a) that $\nabla n_e / n_e = \nabla n_n / n_n + \nabla n_p / n_p \approx 2 \nabla n_n / n_n$, which results, in contrast to Eq. (12b), in an ion distribution that is flatter than the electron distribution (see [24–26] for details). In such a situation (which occurs, e.g., for halogens), the attachment and ionization frequencies are approximately the same, $v_i \approx v_a$, as was noted in [16–18].

which strongly depends on the temperature ratio $k = T_e / T_i$ and coincides with distribution (12b) only in the particular case $T_e = T_i$. The establishment of a Boltzmann distribution for electrons and negative ions at low pressures is illustrated in Fig. 7, in which the simulation results shown in Fig. 3 for a pressure of $p = 0.15$ torr are replotted in accordance with Eq. (17).

Since $k \gg 1$ in the discharge, it follows from Eq. (17) that the electron density profile is nearly flat, $n_e(r) \approx n_{e0} \approx \text{const}$, which is indeed observed at reduced pressures (see Figs. 2, 3). Here, transport processes play a major role in Eq. (3) for the negative ion balance (see Fig. 8), in contrast to the above case with $\tau_{an} v_a > 1$ (cf. Fig. 5). The field-induced and diffusion fluxes of negative ions are almost the same in magnitude, but opposite in sign; hence, a small difference between them is sufficient to balance the production and loss of ions at any point (Fig. 8). The plasmochemical processes govern only the global balance of ions in the central region. In Eq. (2) for the positive ion density $n_p(x)$, the terms on the left-hand side are also approximately equal to each other. However, they are summed up and, thus, at a significant degree of electronegativity ($n_n(0) > n_e(0)$), balance equation (2) for positive ions can be written in the form $-2D_p \Delta n_n = v_i n_{e0}$. This gives a parabolic distribution of the ion densities and a flat profile of the electron density $n_e(r)$ at $r < r_0$ [13–15]:

$$\begin{aligned} n_n(r) &= n_{n0} (1 - r^2 / r_0^2), \\ n_{n0} / n_{e0} &= v_i r_0^2 / 4D_p, \\ n_e(r) &\approx n_{e0} \approx \text{const}. \end{aligned} \quad (18)$$

We note that ion diffusion in the inner region proceeds with the coefficient $2D_p$ of the own ion–ion ambipolar self-diffusion, rather than with the usual coefficient of ambipolar diffusion $D_p(1+k)$. It can be seen from Figs. 2 and 3 that, at low pressures, simple parabolic law (18) for the ion density profiles agrees well with the results of full-scale simulations.²

In the outer region (shell), in which the negative ions are almost absent, the plasma density profile varies in accordance with Eq. (10). In [13–15, 23, 24], the position of the boundary point $r = r_0$ was found from the negative ion balance using model profiles (18). Unfortunately, this procedure is rather laborious and provides a low accuracy. It seems that the position of the boundary can be found in a simpler and more reliable way from the continuity of the positive ion flux at $r = r_0$:

$$2D_p \frac{n_{n0}}{r_0} = \frac{D_p(1+k)n_{e0}}{l_e \tan((R-r_0)/l_e)} \approx \frac{D_p(1+k)n_{e0}}{R-r_0}. \quad (19)$$

² We note also that, in order for profiles (18) to be established, it is enough to satisfy the condition $\tau_{an} v_a < 1$. The mechanism for the volume loss of negative ions, which is determined by the right-hand side of Eq. (3), can be either recombination (at $v_d < K_p n_p$) or detachment (at $v_d > K_p n_p$).

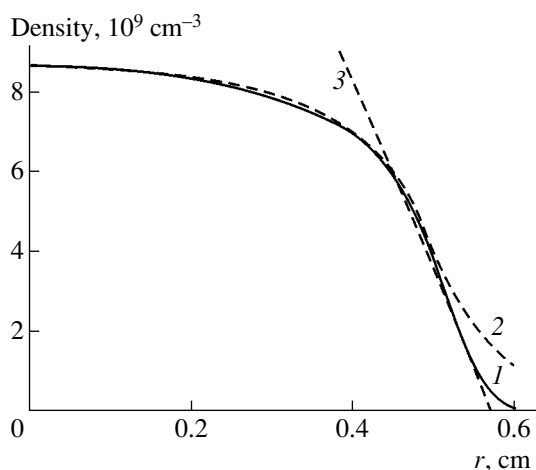


Fig. 7. Boltzmann distributions of electrons and negative ions for $p = 0.15$ torr and $I = 50$ mA: (1) $n_e(r)$, (2) $n_e(0)/[n_n(r)/n_n(0)]^{1/k}$ (see formula (17)), and (3) electron density profile (10) in the outer region.

Model electron density profiles (10) with r_0 defined by Eq. (19) (see Fig. 7) agree well with the results of full-scale simulations shown in Fig. 3.

Based on the analysis performed, we recommend the following procedure to obtain approximate density profiles in the plasma of electronegative gases in the detachment regime ($v_a > K_r n_p$):

(i) First, the parameter $\tau_{an} v_a$ is estimated.

(ii) Then it is necessary to indent from the wall by the thickness δ_{sh} of the space charge sheath, which can be estimated, e.g., according to [26].

(iii) In the outer electron-ion plasma region ($r_0 < r < R$), where $n_p \approx n_e \gg n_n \approx 0$, the electron density varies according to Eq. (10) and the negative ion density varies according to Eq. (15). If $\tau_{an} v_a > 1$, then the thickness of this region is equal to l_e (see Eq. (8)) and the denominator in Eq. (10) is equal to unity ($r_0 = R - l_e$). In the opposite case ($\tau_{an} v_a < 1$), we have $l_e \approx \Lambda$ and the thickness of this region is estimated by formula (19).

(iv) Finally, the density profiles in the central region ($r < r_0$) are determined.

At $\tau_{an} v_a > 1$, the density profiles are similar and are described by Eq. (13), whereas the density values are related by expression (12). Electron density profile (13) is joined to expression (10) at $r = r_0 = R - l_e$. The ion densities undergo a jump at this point: the negative ion density drops to nearly zero (see Eq. (15)), whereas the positive ion density decreases to the value equal to the electron density given by Eq. (10). At $\tau_{an} v_a > 1$, the thickness of the transition zone ($\sim l_n < l_e$) is small and it can be regarded as a jump in the ion density.

At $\tau_{an} v_a < 1$, the electron density profile is flat ($n_e(x) \approx n_{e0}$) and the ion density profile is parabolic. These densities are related by formulas (18). The elec-

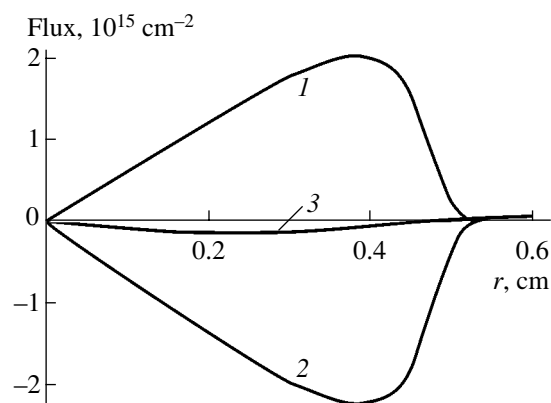


Fig. 8. Contributions of spatial transport and volume processes to the negative ion balance for $p = 0.15$ torr and $I = 50$ mA: (1) the diffusion component of the negative ion flux, (2) its drift component, and (3) the resulting flux balancing the production and loss of negative ions in volume plasmochemical processes.

tron density profile is joined at the point $r = r_0$, whose position can be estimated from Eq. (19).

Thus, using commercial CFDRC software [28], comprehensive simulations of the positive column plasma of a dc discharge in oxygen are performed and the main scaling laws characterizing the spatial distributions of the plasma parameters are determined. The simulation results show that a distinctive feature of the electronegative-gas plasma is that it stratifies into regions with very different ion compositions, so that there are practically no negative ions in the outer electron-ion plasma region (shell). At low pressures ($\tau_{an} v_a < 1$), not only electrons but also negative ions obey a Boltzmann distribution. In the inner region, the electron density profile is flat, whereas the ion density profile is parabolic. In the ion balance, the transport processes prevail; hence, taking into account ion heating dramatically affects the spatial distribution of charged particles. At elevated pressures ($\tau_{an} v_a > 1$), the volume processes dominate in the balance of negative ions and the profiles of the charged particle densities in the inner region become similar to each other.

ACKNOWLEDGMENTS

L.D. Tsandin acknowledges the support of the Russian Foundation for Basic Research (project no. 01-02-16874) and NATO SfP (grant no. 974354).

REFERENCES

1. M. Lieberman and A. Lichtenberg, *Principles of Plasma Discharges and Materials Processing* (Wiley, New York, 1994).
2. H. J. Oskam, *Philips Res. Rep.* **13**, 335 (1958).

3. M. V. Konjukov, Zh. Éksp. Teor. Fiz. **34**, 908 (1958) [Sov. Phys. JETP **7**, 629 (1958)]; Zh. Éksp. Teor. Fiz. **34**, 1634 (1958) [Sov. Phys. JETP **7**, 1122 (1958)].
4. J. B. Tompson, Proc. Phys. Soc. (London) **73**, 818 (1959).
5. H. Sabadil, Beitr. Plasmaphys. **13**, 235 (1973).
6. H. S. W. Massey, *Negative Ions* (Cambridge University Press, Cambridge, 1976; Mir, Moscow, 1979).
7. P. D. Edgeley and A. von Engel, Proc. R. Soc. London, Ser. A **370**, 375 (1980).
8. G. L. Rogoff, J. Phys. D **18**, 1533 (1985).
9. A. V. Phelps, J. Res. Natl. Inst. Stand. Technol. **95**, 407 (1990).
10. L. D. Tsendin, Zh. Tekh. Fiz. **55**, 2318 (1985) [Sov. Phys. Tech. Phys. **30**, 1377 (1985)]; Zh. Tekh. Fiz. **59**, 21 (1989) [Sov. Phys. Tech. Phys. **34**, 11 (1989)].
11. C. M. Ferreira, G. Gousset, and M. Touzeau, J. Phys. D **21**, 1403 (1988).
12. P. R. Daniels, R. N. Franklin, and J. Snell, J. Phys. D **22**, 780 (1989); J. Phys. D **23**, 823 (1990); J. Phys. D **26**, 1636 (1993).
13. A. J. Lichtenberg, V. Vahedi, M. A. Lieberman, *et al.*, J. Appl. Phys. **75**, 2339 (1994).
14. A. J. Lichtenberg, I. G. Kouznetsov, T. D. Lee, *et al.*, Plasma Sources Sci. Technol. **6**, 437 (1997).
15. I. G. Kouznetsov, A. J. Lichtenberg, and M. A. Lieberman, J. Appl. Phys. **86**, 4142 (1999).
16. R. N. Franklin, Plasma Sources Sci. Technol. **11**, 31 (2002).
17. R. N. Franklin and J. Snell, J. Phys. D **32**, 2190 (1999).
18. R. N. Franklin, J. Plasma Phys. **64**, 131 (2000).
19. S. V. Berezhnoj, C. B. Shin, U. Buddemeier, and I. Kaganovich, Appl. Phys. Lett. **77**, 800 (2000).
20. V. A. Feoktistov, V. V. Ivanov, A. M. Popov, *et al.*, J. Phys. D **30**, 423 (1997).
21. V. V. Ivanov, K. S. Klopovsky, D. V. Lopaev, *et al.*, IEEE Trans. Plasma Sci. **27**, 1279 (1999).
22. V. V. Ivanov, K. S. Klopovsky, D. V. Lopaev, *et al.*, Fiz. Plazmy **26**, 1038 (2000) [Plasma Phys. Rep. **26**, 972 (2000)].
23. A. Kono, Appl. Surf. Sci. **192**, 115 (2002).
24. E. A. Bogdanov and A. A. Kudryavtsev, Pis'ma Zh. Tekh. Fiz. **27** (21), 36 (2001) [Tech. Phys. Lett. **27**, 905 (2001)].
25. E. A. Bogdanov, V. I. Kolobov, A. A. Kudryavtsev, and L. D. Tsendin, Zh. Tekh. Fiz. **72** (8), 13 (2002) [Tech. Phys. **47**, 946 (2002)].
26. A. V. Rozhansky and L. D. Tsendin, *Transport Phenomena in Partially Ionized Plasma* (Énergoatomizdat, Moscow, 1988; Taylor & Francis, London, 2001).
27. E. A. Bogdanov, A. A. Kudryavtsev, L. D. Tsendin, *et al.*, Zh. Tekh. Fiz. **73** (8), 45 (2003) [Tech. Phys. **48**, 983 (2003)].
28. <http://www.cfdrc.com/~cfdplasma>
29. E. W. McDaniel and E. Mason, *The Mobility and Diffusion of Ions in Gases* (Wiley, New York, 1973; Mir, Moscow, 1976).

Translated by N. Ustinovskii